JOURNAL OF PROPULSION AND POWER
Vol. 22, No. 4, July–August 2006

Overview of Flow Oscillations in Transonic and Supersonic Nozzles

Henry Y. W. Wong
ESA and Advanced Operations and Engineering Services, 2200 AG Noordwijk, The Netherlands

Nomenclature

A_e/A_*	=	area ratio
A_0	=	admittance function at $x = 0$
a	=	local speed of sound
c, c_m	=	shock velocity and its amplitude
D	=	nozzle diameter
f, f_r, f_p	=	frequency and resonant frequency
$L, L_{\sigma v}$	=	characteristic length scale between shock and nozzle exit
L^*	=	distance between throat and nozzle exit
M	=	local Mach number
$M_{\text{sw}}, M_{\sigma u}$	=	shock wave Mach number
p	=	local static pressure
$\hat{p}_{su}/q$	=	normalized fluctuating static pressure amplitude at top wall
q	=	local mean dynamic pressure
R_{p-x}	=	cross correlation between static pressure and shock location
T	=	one closed-loop time for waves propagating between shock and exit
t_d, τ	=	delay time and nondimensional time
u	=	local velocity
$x/H, x/h$	=	streamwise location from throat and normalized by throat height
$\tilde{\hat{x}}_{\sigma m}$	=	shock motion amplitude normalized by throat height
β	=	reflection coefficient
γ	=	specific heat ratio
Δx_m	=	shock motion amplitude
$\varepsilon, \varepsilon_0$	=	amplification factor behind shock and at nozzle exit
θ	=	half-angle of divergence
κ	=	wave number
ρ	=	local density
ϕ	=	phase angle of reflected wave or between pressure cross correlations or between shock displacement and pressure
ψ	=	phase angle of downstream fluctuating component
ω	=	angular frequency

Subscripts

$e, 3, v, a$	=	nozzle or diffuser exit
j	=	jet
n, m	=	acoustic mode
$t, *$	=	nozzle throat
s	=	shock location
0	=	time-averaged mean value
$1, u$	=	just upstream of shock
$2, d$	=	just downstream of shock

Superscripts

$-$	=	time-averaged mean value
$\prime$	=	fluctuating component
$\sim$	=	normalized by throat height
$\wedge$	=	normalized by values at throat

I. Introduction

THE resonance phenomenon in nozzle flows has been studied in the past by many researchers not only because of academic interest, but also for its significance in many engineering applications ranging from mixing[1] and jet noise control[2] to buffeting in external flows[3] and rocket engine instability.[4,5] The occurrence of resonance can be self-excited or driven by external unsteady loads, or a combination of both mechanisms. For instance, in the case of convergent–divergent (C–D) nozzles without any abrupt change in the cross-sectional area, the nozzles are under a transonic flow condition at a pressure ratio much lower than the design value, and flow separation takes place just downstream of the throat shock. Consequently, self-excited resonance and tones are encountered with such a nozzle flow condition. This kind of phenomenon has been studied experimentally,[6–8] as well as numerically.[7,9] Zaman et al.[6] provide a complete overview of this activity.

In the case of supersonic or hypersonic cold subscaled rocket nozzle flows such as those described by Schwane et al.,[4] flow separation takes place just downstream of a separation shock, free shock separation (FSS), located somewhere between the throat and the nozzle exit inside the overexpanded nozzle, depending mainly on the pressure ratio. A relatively more complex flowfield, restricted shock separation (RSS), can arise if the flow separation reattaches to the nozzle wall downstream of the initial separation location. A detailed account on the flow separation concept related to the side-load behavior of this kind of nozzle can be found by Frey and Hagemann.[10] Under this cold-flow condition, where the movement of the separation shock in the FSS mode is under the influence of external pressure fluctuations at the nozzle exit, amplification of

Henry Y. W. Wong is a senior aerospace engineer at Advanced Operations and Engineering Services in The Netherlands. He is also a consultant to ESA and a member of the European Flow Separation and Control Device Group. H. Wong holds a Ph.D. degree from Cambridge University, England, U. K., and is engaged in research in the field of aerospace propulsion, aeroacoustics, turbulence and secondary flow theories, and computational fluid dynamics. He has published widely in various industry publications. His experience ranges from subsonic cavity flows, to transonic aeroacoustics, to supersonic rocket nozzle flows. He has participated in many ESA projects, including reentry vehicles, satellite aerodynamics, plasma wind-tunnel design, as well as launcher base-flow buffeting. Recently, he has received a long-term engineering service award from AOES and the Achievement Award from Marquis's *Who's Who in Science and Engineering*. He was a scholar from the Science and Engineering Council in England. He is a Senior Member of AIAA.

Presented as Paper 2004-4013 at the AIAA 40th Joint Propulsion Conference, Ft. Lauderdale, FL, 11–14 July 2004; received 9 August 2004; revision received 4 November 2005; accepted for publication 6 November 2005.

fluctuating pressure correlations between the region downstream of the separation shock and the external flow has been reported and studied experimentally[11] and numerically.[4] The shock excursion of this kind of shock movement, which depends on this amplification factor, under certain conditions has a great influence on the side-load effect on the nozzle in the case where flow separation is asymmetric and may pose the threat of the occurrence of structural fatigue of nozzles.

There are other kinds of nozzle flows where resonance phenomenon can be found under a subsonic flow condition, such as those studied by Hill and Greene[1] and Hussain and Hasan[12] in which the nozzle has an abrupt change in the cross-sectional area, sometimes known as whistler nozzles. We shall confine our study mainly to the cases without abrupt area change in the nozzle. However, the relatively more complex resonance mechanisms in this case will be highlighted and compared with those from the other cases.

Another area that is beyond the scope of this study involves a complex interference of tones generated by interactions between disturbances initiated at the nozzle lip and the shear layer at the exit of an underexpanded supersonic jet flow. This induces a resonance phenomenon commonly known as screech tones as reported by Krothapalli and Hsia.[2] Raman[13] has provided a full review and perspective in understanding of the supersonic jet screech. Some comparisons between the nonscreech transonic tone and the screech tone will be shown in this paper.

In addition to highlighting the research and development into the flow oscillation problems achieved in the past, the main objective of this paper is to extend some of the reviews already mentioned, including the latest developments in understanding of the mechanism of resonance phenomena in nozzle flows. The difference and similarity in the characteristics of all of the resonance phenomena reported in this paper will be summarized. In all cases, subject to availability, experimental, numerical, as well as analytical results will be compared and explained.

II. Transonic Diffuser/Nozzle Flows

The motivation of this research originated from the study of flows in airbreathing, supersonic inlets and combustion instabilities in ramjet engines. These studies focused on the response of the terminal shock wave in a transonic/supersonic inlet diffuser to downstream disturbances induced by certain physical flow processes or mechanisms inside a combustion chamber or at the diffuser exit. For the last three decades, most researchers investigated the key mechanisms or processes that governed the shock wave movement. These mechanisms or processes included 1) pressured-gradient-induced separation (PGIS) and shock-induced separation (SIS), 2) periodic shock motion and acoustic resonance, and 3) turbulent boundary-layer and shear-layer instability. The following subsections review and consolidate the results in each of these mechanisms.

A. PGIS and SIS

Two decades ago, Sajben and Kroutil,[8] Chen et al.,[14] and Bogar et al.[15] conducted a series of experimental investigations with a two-dimensional small-angled divergent diffuser at transonic flow conditions. The range of frequencies in those investigations was between 10 and 10,000 Hz with the shock Mach number between 1.1 and 1.4.

Three different flow patterns were investigated, as shown in Fig. 1. In all cases, downstream propagating subsonic waves were initiated at the stems of the throat shock. As a result, self-excited oscillation occurred in the divergent section inside the diffuser. Detailed measurements of unsteady wall pressure and flow separation with miniature, fast-response transducers and oil flow traces, in addition to high-speed schlieren motion pictures for flow visualization of the unsteady shock movement, were conducted and investigated, including the influence of the approach boundary-layer thickness.

At a lower Mach number, less than 1.27, the shock wave pattern was conical and the flow separation was governed mainly by the pressure gradient and, hence, known as PGIS. At a higher Mach number, greater than 1.3, where λ shocks existed near the throat,

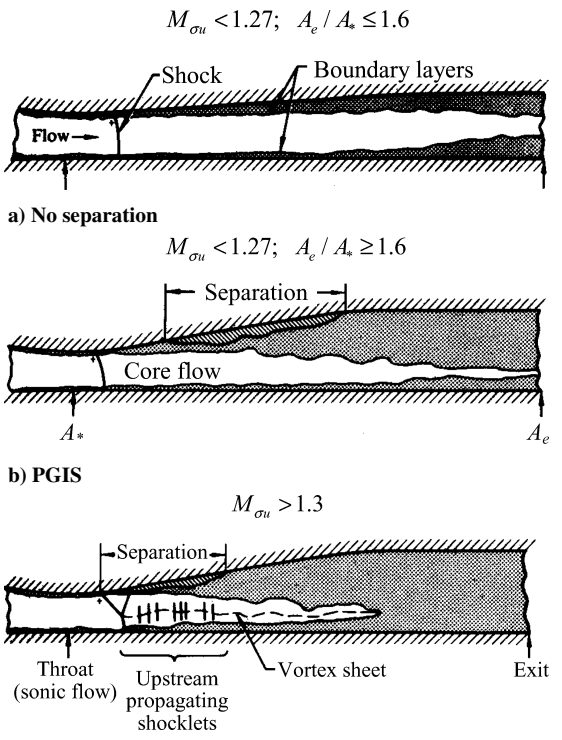

Fig. 1 Typical flow patterns (Bogar et al.[15]).

the flow separation was governed mainly by the strong λ shocks and, hence, known as SIS.

Hunter[7] used a similar two-dimensional nonaxisymmetric experimental configuration in a 16-ft transonic wind-tunnel to conduct an investigation more recently. However, instead of using a flat floor for symmetry, Hunter added the reflected part of the C–D section about the symmetry plane, which had the advantage of testing the symmetry of shock separation. The shock wave Mach number ranged from 1.1 to 2.1. The main objective of his investigation was to understand the static behavior of separated nozzle flows as a first step to resolve the complicated relationship between overexpansion, SIS, and nozzle thrust efficiency.

Hunter did not investigate the difference between the PGIS and SIS modes but found that there were two distinct regimes for SIS depending on the pressure ratio: For a pressure ratio less than 1.8, $M_{sw} < 1.5$, the separation was three dimensional, unsteady, and confined to a bubble; for a pressure ratio larger than 2.4, $M_{sw} > 1.6$, the separation was two dimensional, steady, and fully detached. The transition from the three- to two-dimensional structure in separation was not because of shock–boundary-layer interaction but as a natural tendency of an overexpanded nozzle flow to detach and reach a more efficient thermodynamic balance. Moreover, the Mach flow condition for the existence of the SIS was consistent with that from the Sajben and Kroutil experiment.

The three-dimensional structure in separation was based on the comparison between the side- and the centerline pressure distributions along the wall. Hunter did not report any asymmetry between the top and the bottom flow structures. However, as reported by Meier[16] in his research on shock-induced flow oscillations with a Laval nozzle, the occurrence of an SIS on one wall alone was observed, which indicated the existence of asymmetrical three-dimensional unsteady modes in transonic resonance under certain experimental conditions, as shown in Fig. 2. It will be shown that these conditions include variations of the upstream chamber pressure and the downstream external pressure.

A similar three-dimensional effect for the SIS case was observed in the Bogar et al.[15] experiment as shown in the Mach contours in Fig. 3. Oil-flow traces on the wall indicated the presence of secondary flows directed inward near the reattachment point, causing the influx of low-speed fluid from the sides and increased boundary-layer thickness near the center.

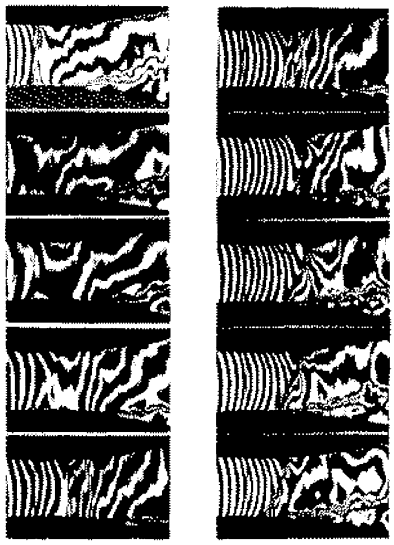

Fig. 2 Interferograms for periodic shock motion in Laval nozzle at $M_{sw} = 1.2$ (Meier[16]).

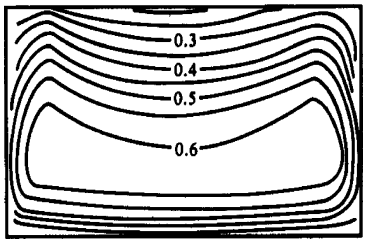

Fig. 3 Mach number contours at exit with $M_{\sigma u} = 1.35$ (Bogar et al.[15]).

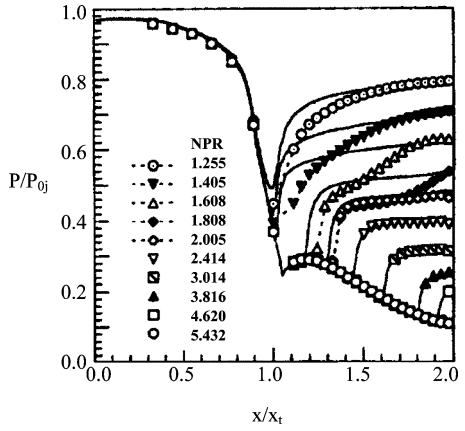

Fig. 4 Normalized pressure profiles along centerline with various PRs (Hunter[7]).

Hunter,[7] in addition to his experimental investigation, performed computational fluid dynamics (CFD) calculations on his two-dimensional C–D nozzles with a time-averaged Navier–Stokes solver coupled with $\kappa-\varepsilon$ turbulence closure and nonlinear algebraic Reynolds stress models. A wall-tripped point was located near the inlet of the inflow duct to form a turbulent boundary layer in the test nozzle. A large number of pressure ratios (PRs) ranging from 1.25 to 8.78 were calculated for a detailed comparison with his experimental data, including the schlieren images. At low PRs, PR ≤ 2.4, the comparison of the wall static pressure along the centerline between the experimental data and the CFD results was rather crude as shown in Fig. 4. This was mainly because of the three-dimensional effect in the flow structure, as mentioned earlier, and partly because of the unsteadiness in the flowfield, which the two-dimensional steady computations neglected. At high PRs, the comparison was in good agreement because the flow was two dimensional and steady, satisfying the computation conditions.

B. Periodic Shock Motion and Acoustic Resonance

Periodic shock motion existed in both PGIS and SIS modes. In the experimental investigation described in Sec. II.A, Sajben and Kroutil,[8] Chen et al.,[14] and Bogar et al.[15] showed that multiple peaks in the wall pressure power spectral densities (PSDs) downstream of the shock were observed at low PRs with the PGIS mode as a result of the longitudinal duct acoustical resonances with fundamental and odd harmonics at low frequencies, ~100 Hz, as shown in Fig. 5.

Hunter[7] also observed the periodic motion of the shock just downstream of the nozzle throat with the SIS mode in the schlieren flow-visualization experiment. According to Zaman et al.,[6] an audio signal from a microphone was recorded simultaneously during the Hunter schlieren experiment, which showed multiple modes of resonant frequencies as shown in Fig. 6.

Szumowski et al.[17] measured similar oscillation modes in an unsteady Laval nozzle flow experiment. Each mode was associated with a particular shock pattern and the behavior of the flow separation. Ishibashi and Takamoto,[18] in their research of discharge coefficients of critical nozzles (axisymmetric quadrant and Venturi nozzles), demonstrated the existence of standing waves in the measurement of the recovery temperature with a thin thermocouple inside the divergent section of the nozzle. The PR was two with a core subsonic outflow downstream of the throat.

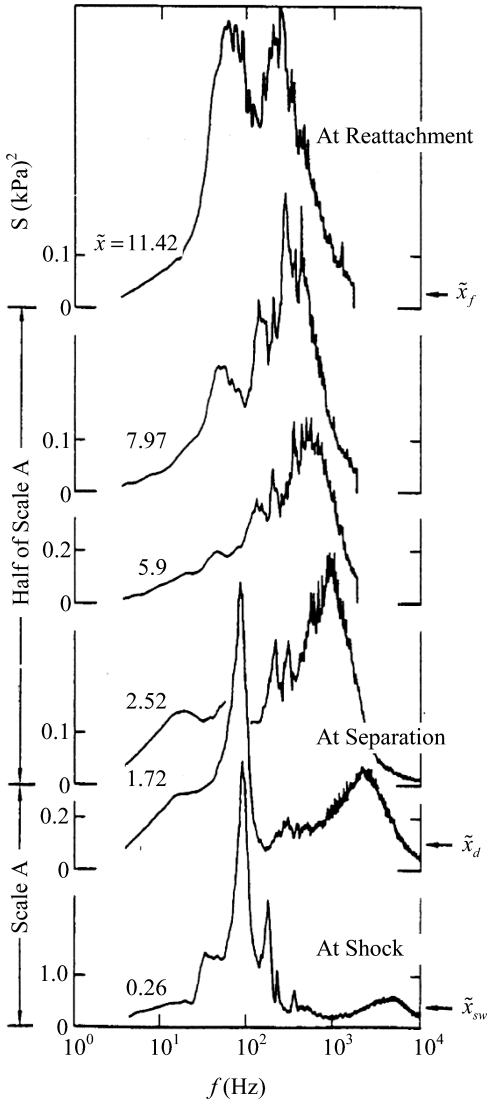

Fig. 5 Top wall pressure PSDs for $B = 2.8\%$ and $M_{sw} = 1.2$ (Sajben and Kroutil[8]).

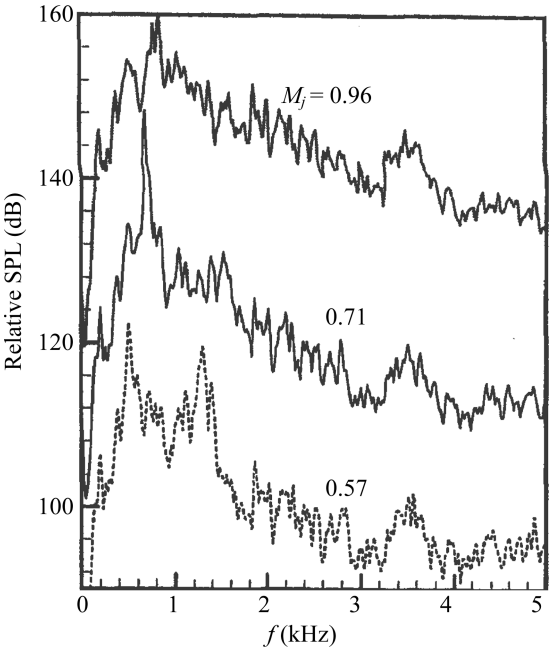

Fig. 6 Sound pressure spectra from Hunter experiment (Zaman et al.[6]).

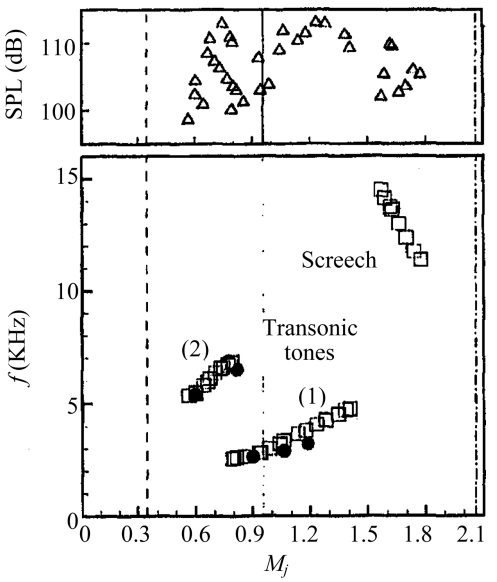

Fig. 7 Variation of □, frequency and △, amplitude of tones with jet Mach number for nozzle, $D_t = 0.3$, $D_e = 0.4$, and $L_{te} = 0.75$ in. (Zaman et al.[6]).

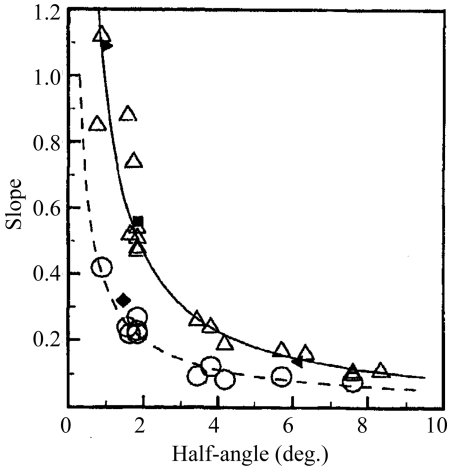

Fig. 8 Variation of slope of fL_{te}/a with M_j for various nozzles as function of θ (Zaman et al.[6]).

Zaman et al.[6] launched a series of experimental investigations with three jet facilities of different sizes (30, 10, and 5 in. or 76.2, 25.4, 12.7 cm in plenum chamber diameter), (0.635 to 8.89 cm in exit diameter) where, in each facility, compressed unheated air inside a cylindrical plenum chamber was discharged through the nozzle into the quiescent ambient. The nozzles, 16 in total, were designed to include three-dimensional circular and two-dimensional rectangular shapes with sizes ranging from $\frac{1}{4}$ to $3\frac{1}{2}$ in. in exit diameter and to include similar scales in the axial length. In all cases, the half-angle of divergence θ was less than 9 deg, with some nozzles made of aluminum and some of transparent plastic. The set of plastic nozzles, seven in total, was devoted to the frequency-scaling study. The main objectives were 1) to advance the understanding of the resonance phenomenon, 2) to predict its frequency, and 3) to find a method to suppress its occurrence. Detailed measurements, both in the axial and radial directions, of the static pressure, total pressure, and wall temperature were conducted. In addition, audio signals similar to those taken in the Hunter experiment were recorded to test the boundary-layer trip effect.

Zaman et al. concluded that transonic resonance occurred with the presence of a shock in the divergent section of the nozzle. The resonant frequencies appeared in multiple modes, with the fundamental mode corresponding to a standing wave of a quarter-wavelength at a high PR (1.7–3.2); higher modes existed only in odd harmonics at a low PR (1.4–1.7 for second and 1.2–1.4 for third) as shown in Fig. 7. Different from the Hunter experiment, only axisymmetric unsteady shock motion was observed. Moreover, the resonant frequencies f_r were strongly dependent on the divergent angle of the nozzle for θ smaller than 2 deg, as shown in Fig. 8, based on which an empirical correlation between f_r and θ was derived.

The steep gradients in the region below $\theta = 2$, deg as shown in Fig. 8, can be explained by the sensitivity of the change in the distance between the shock and the nozzle exit, which is the characteristic length scale L in the determination of the resonant frequency. This can be shown in the analytical investigation of the shock motion and acoustic wave interaction.

We begin with the work of Burgers,[19] who examined the transmission and reflection of waves with phase fronts parallel to a plane shock wave moving in a uniform gas medium. That was essentially the interaction between a normal shock and an acoustic wave approaching the shock in a channel with a constant cross-sectional area. Independently, Kantrowitz[20] analyzed the stability of shock waves in a nonuniform channel. Both researchers established a foundation for the stability of a shock wave under a perturbed disturbance of acoustic waves generated by an external source. Hurrell[21] employed the same technique to determine the relaxation time τ of a normal shock, under an initial finite duration of a periodic oscillation in a diverging channel. The results showed that the shock displacement decayed to zero if τ was positive and grew indefinitely if τ was negative. Consequently, the main conclusion was that a normal shock was stable in a divergent channel and unstable in a convergent channel. This conclusion is consistent with all of the experimental observations reported so far. Wasserbauer and Walloh[22] contributed the idea of using the periodic shock motion as a boundary condition in the analysis of a nonuniform subsonic duct with a supersonic inlet. The results agreed with their measurements, which justified the validity of the periodic shock motion in the inlet as a first-order accurate result. Despite the different flow conditions, this is similar to the periodic shock motion observed in the Hunter experiment as well as in the numerical results from Loh and Zaman.[9] Richey and Adamson[23] and Adamson et al.[24] demonstrated a second-order accurate nonlinear shock motion by applying a potential theory to the response of shock motion to a periodic disturbance in a two-dimensional transonic channel flow.

Culick and Rogers[25] extended the work of Hurrell[21] and followed the approach of Burgers[19] and Kantrowitz,[20] but used a diverging

channel to develop a model that fitted most easily into an approximate analysis of ramjet engines. It is relevant to elaborate their results here because their results come close to what we are searching for in the development of the resonance phenomena in nozzles. They employed the model of Wasserbauer and Walloh for the inlet boundary condition. Furthermore, they assumed quasi-steady behavior in the shock motion relative to a weak acoustic wave, propagating upstream toward the shock and reflecting downstream away from the shock. The amplitude in the shock displacement was assumed small. Based on those assumptions, Culick and Rogers linearized the acoustic equations, which yielded the magnitude and phase of the reflected wave in terms of the admittance function A_0, where

$$A_0 = \bar{\rho}\bar{a}\left(\frac{u'}{p'}\right) \tag{1}$$

$$|\beta| = \left[\frac{(1+A_{0r})^2 + A_{0i}^2}{(1-A_{0r})^2 + A_{0i}^2}\right]^{\frac{1}{2}} \tag{2}$$

$$\tan\phi = \frac{2A_{0i}}{1-\left(A_{0r}^2 + A_{0i}^2\right)} \tag{3}$$

$$\tan\psi_p = \frac{-\sin Kx + |\beta|\sin(Kx+\phi)}{\cos Kx + |\beta|\cos(Kx+\phi)} \tag{4}$$

$$\tan\psi_u = \frac{\sin Kx + |\beta|\sin(Kx+\phi)}{-\cos Kx + |\beta|\cos(Kx+\phi)} \tag{5}$$

$$K = \frac{k}{1-\bar{M}^2} \tag{6}$$

Equations (1–6) form part of a complete set of solutions for the acoustic field in the inlet uniform duct. The equations relating the fluctuating components to the admittance function, which will be important for the determination of the rms pressure and velocity amplitudes, may be found in Ref. 25. For the discussion of the resonant frequency f_r, Eqs. (1–6) would be sufficient because, as will be shown later, f_r is independent of the amplitude of fluctuation but dependent mainly on the relative phase between propagating waves. Based on the preceding assumptions, Culick and Rogers evaluated the admittance function in two limits, where one represented isentropic flow on both sides of a shock wave and the other yielded an approximation to the influence of flow separation induced by the shock wave. In both cases, the admittance function was a complex function of the local time-averaged velocity, pressure, speed of sound, and Mach numbers, upstream and downstream of the shock, and a dimensionless frequency. We shall not reproduce the formulas here because of their complexity.

Culick and Rogers concluded that, in the no-separation case, under the action of an oscillating pressure, the normal shock wave remained stable in a diverging channel, which confirmed Hurrell's results; the shock wave acted to dissipate acoustic energy by attenuating oscillations. In the SIS mode, there was a broad band of low frequencies at high Mach numbers $M_1^2 > (\gamma+3)/2$ such that the shock wave acted to drive the oscillations (unstable), which could eventually induce formation of λ shocks. Moreover, the analysis was weakly extended to second order to demonstrate the result from Richey and Adamson[23] and Adamson et al.[24] that asymmetric nonlinear shock motion existed.

However, there are some uncertainties in this analysis. The ignorance of the influence of the three-dimensional shock structure and the assumed uniformity in the flow properties downstream of the separation are the most significant simplifications in this one-dimensional analysis. Any nonuniformity in the inlet could cause some unknown uncertainties in the results. Moreover, flow separation is never a one-dimensional phenomenon. Furthermore, unsteady nonacoustic fluctuations, because of the flow separation, have not been included in the analysis. The order-of-magnitude in these fluctuations relative to the shock movement is not known. In addition to these uncertainties, this analysis is limited in that it is only valid for a very low frequency, effectively $f \sim 0$.

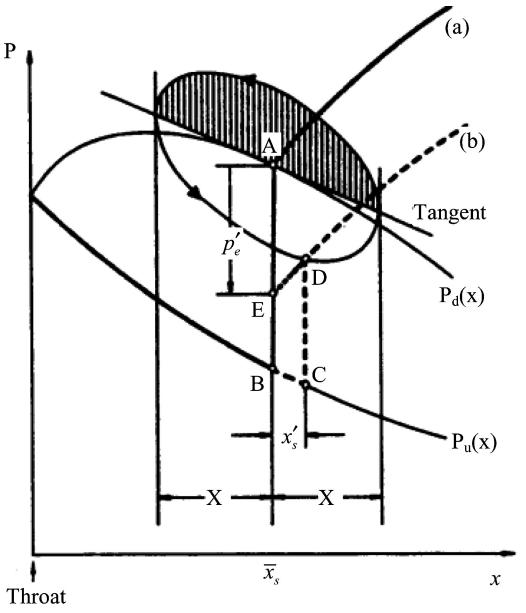

Fig. 9 Elliptical trajectory of pressure distributions downstream of a shock with periodic oscillation (Sajben[26]).

Sajben[26] extended the analysis of Culick and Rogers to be valid for a finite frequency. In addition, Sajben derived an expression for the relationship between the pressure just downstream of the shock and the shock displacement as an ellipse, as shown in Fig. 9. However, the size of the ellipse was the shock excursion, which was an unknown function of the amplitude and frequency of the acoustic disturbance source just downstream of the shock. Sajben did not elaborate further on the relationship between the relative phase and frequency of the periodic fluctuation, but merely illustrated the frequency effect on the relative phase and amplitude of the pressure downstream of the shock and of the shock displacement.

Bogar et al.[15] derived the natural (resonant) frequencies for their PGIS mode experiment where the shock reflected weakly to the acoustic wave propagating upstream toward the shock. The method was based on superpositioning two acoustic waves that were identical but traveling toward each other. The resonant frequencies were predicted as

$$f_n = \left[\frac{2n-1}{4} - \frac{\phi_n}{4\pi}\right] \Bigg/ \int_{x_{\text{shock}}}^{x_{\text{exit}}} \frac{\mathrm{d}x}{a(x)[1-M^2(x)]}$$

$$n = 1, 2, 3, \ldots \tag{7}$$

$$T_n = 2\int_{x_{\text{shock}}}^{x_{\text{exit}}} \frac{\mathrm{d}x}{a(x)[1-M^2(x)]} + \frac{\phi_n}{2\pi f_n} \tag{8}$$

$$f_n T_n = \frac{(2n-1)}{2} \tag{9}$$

where the phase shift between the two waves was evaluated by the Culick and Rogers theory as already mentioned, but based on the measured natural frequencies. The comparison between the theory and the measurement was good, as shown in Fig. 10, which justified that the resonant phenomenon was caused by the mechanism of superpositioning the downstream propagating acoustic waves generated by the shock and the upstream propagating acoustic waves reflected at the diffuser exit. The resonant frequency was inversely proportional to the distance L between the shock and the diffuser exit. This result is consistent with the empirical result obtained by Zaman[6] as described in the experimental investigation.

Handa et al.[27] proposed evaluating the shock displacement by employing the Culick and Rogers theory in the development of the admittance function for the attached flow case, but ignoring the interference of the reflected wave from the shock given by Eqs. (1–6). From the shock displacement equation, Handa et al.

found the resonant frequency, which maximized the shock displacement, to be

$$\max\left\{\frac{(C\varepsilon\hat{p}_2)^2\hat{f}}{2\left[1+(2\pi\hat{f}\hat{\tau})^2\right]}\right\}, \qquad \hat{f}_p = 1/2\pi\hat{\tau} \tag{10}$$

where C was a mean flow constant and $\hat{\tau}$ was first-order nondimensional time, dependent only on the mean flow properties. Equation (10) was compared with the Sajben and Bogar et al. experimental data, as shown in Fig. 11. The comparison seemed reasonable but not rigid enough to support the conclusion from Handa et al. that the occurrence of the resonance phenomenon in the Sajben experiment was governed purely by the geometry shape of the diffuser and the Mach number upstream of the shock.

There are a few uncertainties in this analysis. First, according to Fig. 11, the comparison is not very convincing in terms of the number of results and the deviation of the slope of the curve from the experimental data. Second, in Eq. (10), the assumption of the amplification factor ε independent of the frequency could be incorrect. On the other hand, the Bogar et al. theory shown in Fig. 10 contains a large number of experimental data, and both the values and the slopes of the data are in line with the theory. Moreover, there is no indication in the Handa et al. theory to predict the higher harmonics other than the fundamental mode.

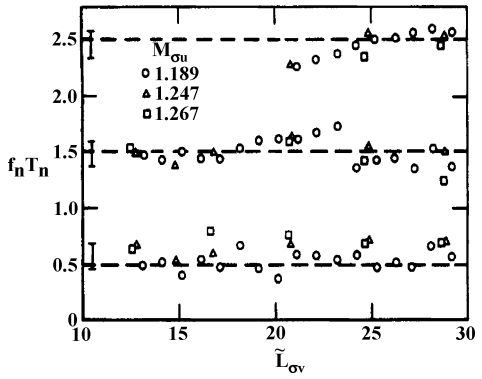

Fig. 10 Normalized resonant frequencies for flows with PGIS mode at various diffuser lengths (Bogar et al.[15]).

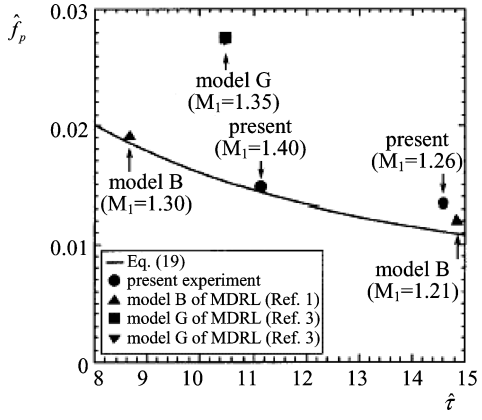

Fig. 11 Peak frequency vs normalized time (Handa et al.[27]).

Recently, Wong[28] considered an inviscid conical nozzle flow with a small angle of divergence. A conical shock was generated inside the nozzle for a given PR. The shock was induced to oscillate under the influence of a small-amplitude periodically fluctuating pressure at the nozzle exit. The periodic boundary at the shock was similar to the approach taken by Culick and Rogers for the inlet as mentioned earlier. The periodic boundary at the nozzle exit was similar to the C–D nozzle flow, which was justified by the numerical results from Loh and Zaman.[9] By solving a one-dimensional wave equation in the subsonic domain downstream of the shock subject to the two periodic boundary conditions (dual-oscillator concept), in the first part of his analysis with a strongly reflected wave, Wong independently established a relationship between the resonant frequency and the characteristic length scale L between the shock and the nozzle exit as

$$f_r = \frac{(2m+1)\left(a^2-u_{30}^2\right)}{4aL} \tag{11}$$

$$\phi = n_\phi\pi, \qquad n_\phi = 0 \text{ or } 1 \tag{12}$$

where u_{30} was the mean velocity at the nozzle exit. The phase angle ϕ was a multiple of π independent of the amplitude of the pressure fluctuation at the nozzle exit. The phase angle of the fluctuating pressure wave at the nozzle exit ψ_p was identical to Eq. (4) given earlier from Culick and Rogers.

A comparison between Eq. (11) and the experimental data from Zaman et al.[6] and Sajben and Kroutil[8] is shown in Table 1. The prediction from the theory is within the range in f_r given by the experiments with different PRs except in a few cases where the divergence angles are large. One of the uncertainties in the comparison is the selection of a correct length scale. L^* is not the correct length scale, but it is the only length scale available for an estimation of L. The mean velocity downstream of the shock in the subsonic domain is also not available. In the two-dimensional diffuser, the correct length scale is not L^* but the distance between the shock and the location where the flow gradient changes significantly that induces the wave reflection. These uncertainties, together with the two- or three-dimensional effects in case of a large θ, cause the discrepancy in the comparison.

For a small-angle-of-divergence nozzle, Eq. (11) is asymptotic to Eq. (7) from Bogar et al. except for the phase angle, the value of which Bogar et al. estimated based on the Culick and Rogers admittance function A_0 at the measured resonant frequencies. In the case with a strongly reflected wave, A_0 becomes very small ($\ll$1), and, according to Eq. (3), the phase angle tends to become Eq. (12). In addition, Eq. (12) is valid for any case with a real A_0. The importance of the Wong approach is not to confirm the semiempirical results of Bogar et al. and Zaman et al., but to identify analytically the significance of the characteristic length scale L to the prediction of the resonant frequency that most researchers in the past have realized only based on the experimental data. A difference in the separation shock location, which could be strongly influenced by the PR, turbulent boundary layer, and Reynolds effect especially in nozzles with a small divergent angle, renders a difference in the resonant frequency.

However, Eqs. (7) and (11) do not include the damping effect generated downstream of the shock in the subsonic domain. This

Table 1 Comparison between one-dimensional theory and experiment in resonant frequency (Wong)

Nozzle	Throat-exit length L^*, m	Divergence angle θ, deg	Resonant frequency f_r, kHz	
			Experiment	Theory
2T2[a]	0.038	1.83	2–5	2.2
5T1[a]	0.107	6.35	0.3–0.6	0.8
6T2[a]	0.019	0.76	4–7	4.5
1T1[a]	0.0095	8.34	3–5	8.9
McDonnell Douglas two-dimensional Diffuser[b]	0.551	8.8	0.1–0.15	0.15

[a]NASA John H. Glenn Research Center C–D three-dimensional nozzle (Zaman et al.)., [b]Sajben and Kroutil.

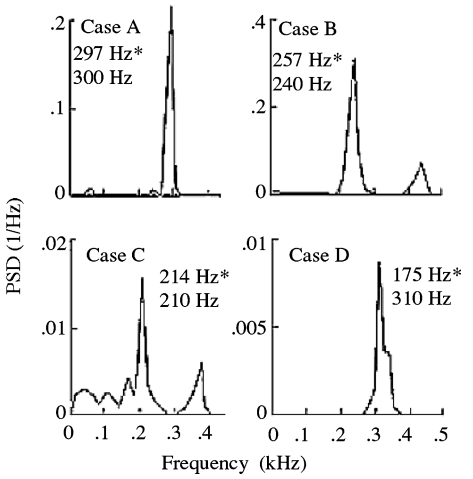

Fig. 12 PSD distribution for wall pressure, cases A–D, x/H: 8.66, 10.06, 12.08, and 14.77, where asterisks indicate one dimensional theory (Wong) results (Hsieh and Coakley[30]).

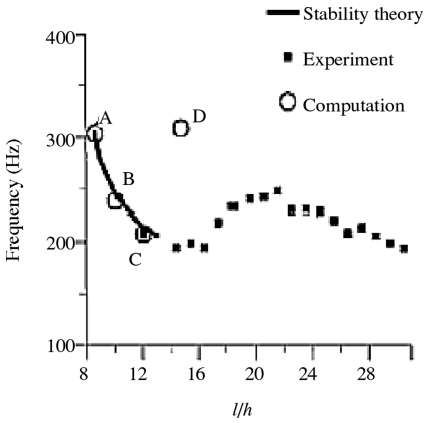

Fig. 13 Frequency (hertz) vs normalized diffuser length (Robinet and Casalis[31]).

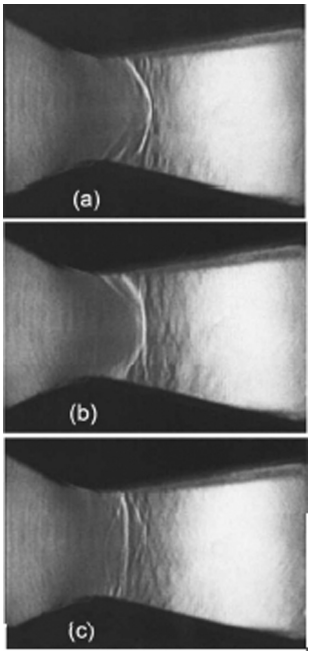

Fig. 14 Schlieren shock structure at different times for fundamental mode in two-dimensional diffuser (Hunter[7]).

has a significant influence to the resonance phenomenon in the case where the correlation between compressibility and fluctuating velocity and the fluctuated kinetic energy in the convection are not negligible compared with the energy generated by the pressure fluctuation in the subsonic domain. This will be shown in more detail later for the supersonic case, where the second part of the analysis of Wong[28] will be highlighted.

Liou and Coakley[29] did the crosschecking for the Sajben[8] experiment with a time-dependent Navier–Stokes solver coupled with a κ–ω^2 turbulence model. The calculation reproduced the periodic shock motion with a single distinctive frequency 50% higher than the measured frequency but failed to detect the multiple peaks observed in the experiment. Hsieh and Coakley[30] improved the prediction by studying the effect of the location of the downstream boundary condition. The extension of the diffuser downstream boundary significantly reduced the frequency and amplitude of oscillations for pressure, velocity, and shock movement, as shown in Fig. 12. The extension of the diffuser length implied a longer acoustic characteristic length scale L, which rendered a lower resonant frequency according to Wong's[28] one-dimensional theory. However, contrary to the conclusion from Hsieh and Coakley, which was based on a comparison with an incorrect half-wavelength acoustic theory, Wong showed that cases A–D provided acoustic resonant frequencies. Moreover, the sudden unexpected increase of the resonant frequency at the location farther downstream from case D (longest L) could be related to the influence of turbulence (see also Sec. II.C) and the suction slots to the local boundary-layer thickness, as well as to the local mean flow velocity. These factors have a significant effect to the resonant frequency prediction according to Wong.[28]

Robinet and Casalis[31] tackled the transonic diffuser problem by applying a quasi-one-dimensional linear stability theory to a CFD solution of the time-averaged Navier–Stokes equations. The objective was to determine how the flow behaved under an infinitesimal perturbation in the mean flow. The sign of the temporal amplification growth rate characterized the stability. The result in the resonant frequency was consistent to the Bogar et al. experimental data and the Hsieh and Coakley numerical solution, as shown in Fig. 13.

However, the major drawback of this approach is the assumption of the existence of a core flow at the diffuser exit, which contradicts the flow condition in the Bogar et al. experiment (Fig. 1) for the case shown in Fig. 13. Moreover, the method is semi-empirical in the sense that the shock motion spectrum is related to the fluctuating pressure by a parameter ε depending on the experimental data. This parameter ε could be a function of frequency as described by Wong[28] but was regarded as frequency independent in the theory. Furthermore, the assumption of a uniform streamwise-independent mean flow in the vicinity of the shock is not justified in this perturbed unsteady flow problem.

Loh and Zaman[9] employed a space–time conservation-element and solution-element (CE/SE) numerical method to study two-dimensional axisymmetric C–D nozzle transonic flows. The CE/SE nonreflecting boundary conditions (NRBC) were implemented in the Navier–Stokes solver, which was coupled with a large eddy simulation (LES) subroutine for turbulence assessment in the jet shear layer outside the nozzle exit. The nozzle length was 0.75 in. with $\theta = 3.81$ deg corresponding to one of the nozzle test cases (3T2) as described by Zaman et al.[6] Grid resolution was studied with several different PRs ranging from 1.28 to 2.39. Figure 7 shows the comparison between the numerical prediction (black dots) and the experimental data from Zaman et al. The trend of frequency variation within each mode and the resonant frequencies were in reasonable agreement with the experimental data from Mach 0.9 to 1.2. However, there was still some uncertainty in the comparison at Mach 1.5. In addition, the periodic variation of the shape and structure of the shock were predicted similar to those observed by Hunter[7] with a two-dimensional rectangular diffuser, as shown in Fig. 14.

Because of the discontinuity in the boundary condition at the nozzle exit, any subsonic downstream traveling longitudinal wave initiated from the separation shock has a reflection at the exit and travels back upstream through the subsonic stems of the shock. The wave propagation continues upstream of the shock within the subsonic boundary layer until a reflected wave takes place. It is the superposition of the azimuthally coherent upstream and downstream

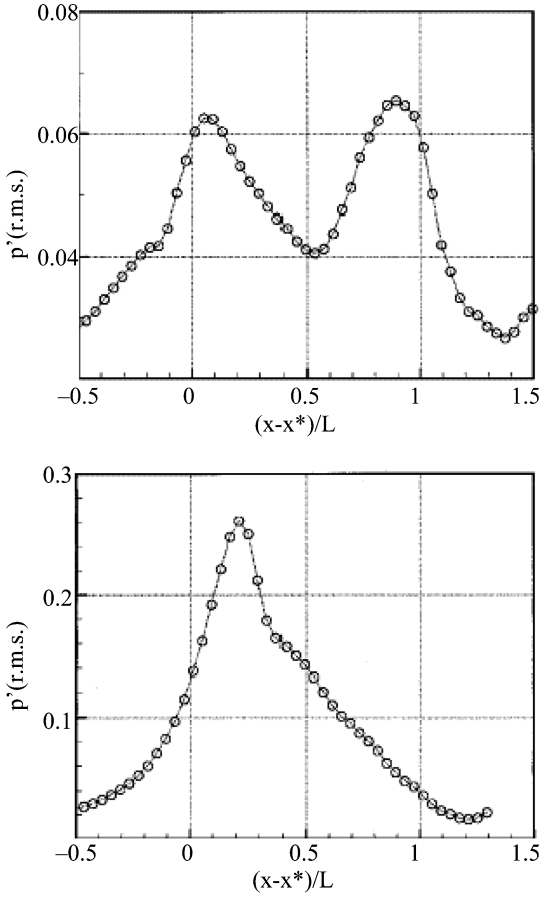

Fig. 15 Fluctuating pressure amplitude (rms) along nozzle centerline at PR = 1.278 (third harmonic) and PR = 1.694 (first harmonic) (Loh and Zaman[9]).

traveling waves that generates the acoustic resonance with multiple nodes and antinodes, including a pressure antinode at or close to the shock and a node close to the exit. The distance between a node and an antinode very much depends on the resonant frequency. Figure 15 shows the computed rms pressure fluctuation along the centerline of the nozzle, clearly exhibiting the fundamental mode and the third harmonic of the resonant frequencies.

Moreover, the computations showed that the effect of a high and a moderate Reynolds number on the resonant frequency was less than 2%. Despite the good agreement in the resonant frequencies with the experimental data, there was still uncertainty in the influence of the turbulent boundary layer in the nozzle, which the solver neglected and regarded as inviscid layers, contrary to the approach by Hsieh and Coakley. There was no comparison with the experimental data in the pressure fluctuating amplitude. The significant influence of the turbulent boundary layer downstream of the shock to the resonant frequency, as mentioned by Handa et al.[27] in the experimental investigation of the two-dimensional diffuser (see Sec. II.C) was not reflected in the two-dimensional axisymmetric nozzle.

C. Turbulent Boundary-Layer and Shear-Layer Instability

Sajben and Kroutil,[8] Chen et al.,[14] and Bogar et al.[15] showed experimentally, as described in Sec. II.A, that one or two peaks in the wall pressure PSDs occurred near the divergent exit as a result of the local turbulence in the shear layer with a frequency ranging from ~300 at the exit to ~6000 Hz at the shock. In addition, a single strong peak in the shock motion PSD was found at high PRs, $M_{\sigma u} = 1.35$, with the SIS mode independent of the duct acoustic effect. However, when the approach boundary layer was thickened, the shock excursion was increased significantly in the PGIS mode but insignificantly in the SIS mode.

The cause of this strong peak in the shock motion PSD at high PRs $M_{\sigma u} = 1.35$, with the SIS mode, was not understood. The amplitude of this strong peak, both in the shock motion and the pressure fluctuation at the shock, as shown in Fig. 16, was one order-of-magnitude larger than the corresponding peaks in the PGIS mode at $M_{\sigma u} < 1.27$. Bogar et al. proposed that it could be related to the effect of the highly turbulent, separated boundary layers interacting with the acoustic waves propagating downstream from the shock and that was independent of the acoustic reflection at the diffuser exit. This is consistent with the failure of the one-dimensional acoustic model from Wong[28] to explain the SIS mode.

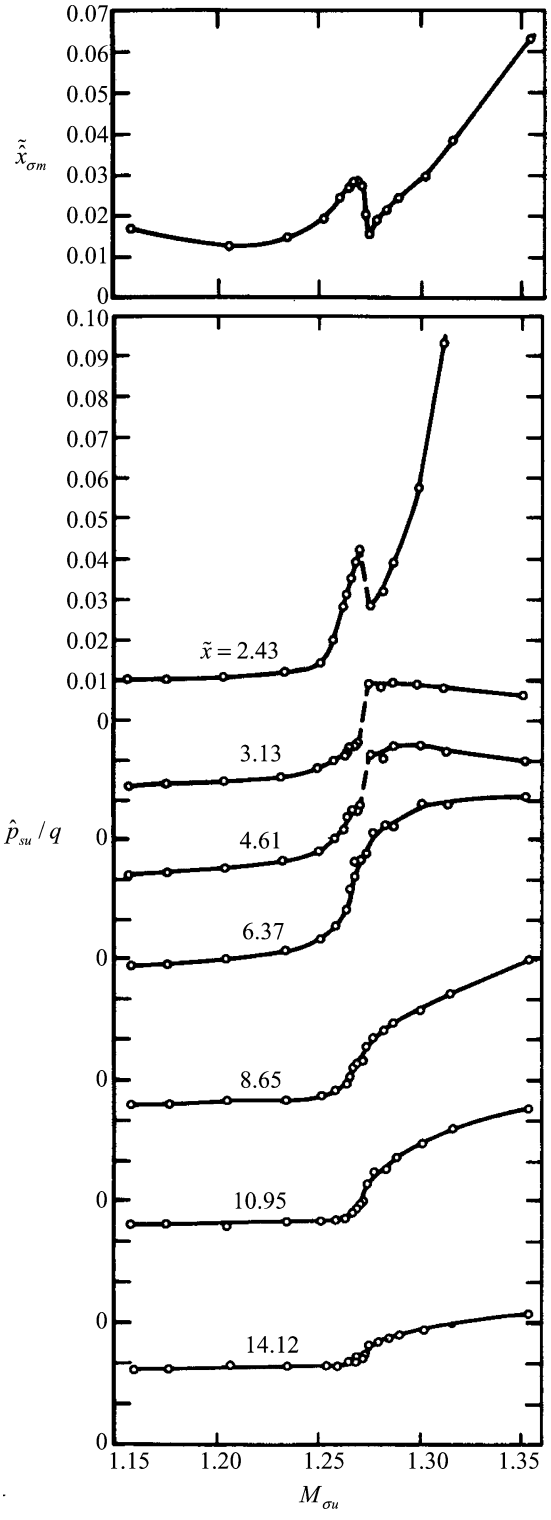

Fig. 16 Unsteady shock motion and top wall pressure amplitudes (Bogar et al.[15]).

In the PGIS mode, according to the results shown in Fig. 5, the turbulence effect at high frequencies near the duct end did not seem

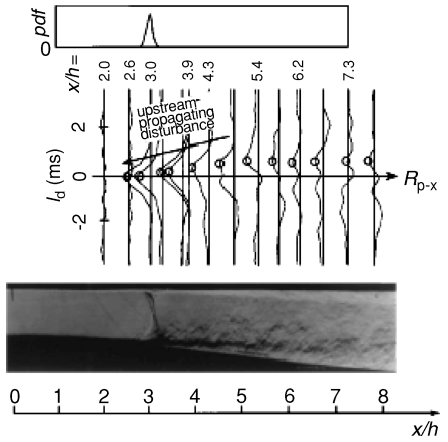

Fig. 17 Cross-correlation coefficients of top wall static pressure with shock displacement at $M_{sw} = 1.48$ (Handa et al.[27]).

to interact with the shock oscillation at low frequencies. In the Bogar et al.[15] experiment, the acoustic wave was weakly reflected at the shock, the high-frequency turbulence near the duct end was absent, and the resonance amplitude was relatively lower compared with that from Sajben and Kroutil[8] because of the absence of the high-energy turbulence at frequencies near the shock frequencies.

Recently, Handa et al.[27] repeated the Sajben experiment with a subscaled two-dimensional transonic diffuser. The shock excursion in the diffuser and the static pressure fluctuations along the flat wall were measured simultaneously. The relative humidity of the air in the plenum chamber was reduced to prevent the possible occurrence of condensation in the test section. Condensation could cause an unwanted wall pressure increase or even postpone the flow separation downstream, which will be addressed further in the section on hypersonic nozzle flows. The Mach number M_{sw} ranged from 1.26 to 1.48. Cross-correlation coefficients between the static pressures on the sidewall and between the top wall static pressure and the shock displacement, as shown in Fig. 17, were measured.

Based on those measurements alone, Handa et al. concluded that, in the PGIS mode, a pressure disturbance was generated near the stem of the shock on the curved wall in the divergent section because of the boundary-layer separation and was convected downstream. In addition, a pressure disturbance was generated at a streamwise cross section, where the unsteady boundary layer downstream of the shock became highly turbulent, and the disturbance propagated upstream, which caused the oscillation of the shock (broad PSD, Fig. 5) as shown in Fig. 17.

The experiment did not cover the SIS mode (narrow PSD), which Bogar et al.[15] measured as a single strong peak independent of the nozzle length. However, the Mach number and the flow separation behaved more like the SIS mode than the PGIS mode. Moreover, it was rather unclear that the pressure disturbance propagating upstream, which occurred mainly along the upper wall, was because of the unsteadiness in the boundary layer, or because of the rapid change in the boundary-layer thickness that rendered an acoustic reflection. Nevertheless, a turbulent boundary layer downstream of the shock could induce oscillations and acoustic resonance in the shock movement independent of the nozzle length.

In addition to the experimental investigation, Handa et al.[27] employed a quasi-one-dimensional Euler solver with the second-order symmetric total variation diminishing (TVD) scheme[32] to test the response of a shock wave interacting with a pressure disturbance traveling upstream toward the shock inside the two-dimensional diffuser. White noise was imposed in the flow at the location where the amplitude of the static pressure fluctuations was highest. The amplitude of the disturbance was determined from the condition that the calculated amplitude of the shock wave oscillation matched with the experiments. The downstream boundary condition was set to have no disturbance wave reflection. Moreover, the Mach numbers used in the calculations were slightly different from those taken in the experiments because of ignorance of the boundary layer in the Euler solver. The Mach numbers were selected to have the time-averaged

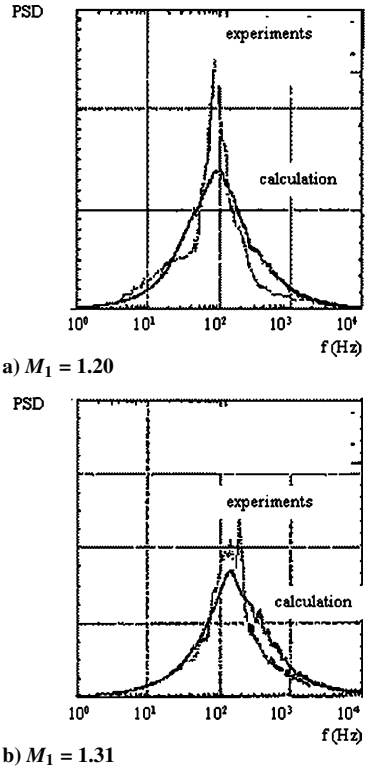

Fig. 18 PSD shock wave displacement for Sajben experiment with 2% inlet blockage (Handa et al.[27]).

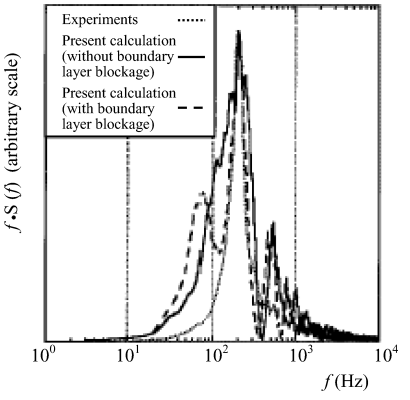

Fig. 19 PSD shock wave displacement for Bogar experiment (Handa et al.[27]).

shock locations matching with those from the experiments. A PSD of the shock displacement comparison was made with the Sajben experiment, as shown in Fig. 18. The agreement between the experimental data and the numerical prediction was good for the resonant frequency but not quite as good for the amplitude. However, there was some adjustment in the calculated intensity over the range of frequencies measured, in addition to the Mach number adjustment as mentioned earlier, to fit with the experimental data. All of the adjustments could have reduced confidence in the numerical prediction. Nevertheless, based on those comparisons, Handa et al. concluded that, in the two-dimensional diffuser, such as the one in the Sajben experiment, the pressure disturbance due to the wave reflection at the exit was small in comparison to that due to the turbulent boundary layer downstream of the shock, in the determination of the shock wave oscillation. In the case of the Bogar et al. experiment, Handa et al. suggested that the resonant frequency was mainly the result of the acoustic reflection at the exit. For that reason, the downstream boundary condition was set to allow disturbance wave reflection. A PSD of the shock displacement comparison was made with the Bogar et al. experimental data, as shown in Fig. 19. Handa et al. could not explain why peaks other than that at 200 Hz were not observed in the experiments. On the other hand, it was not clear why,

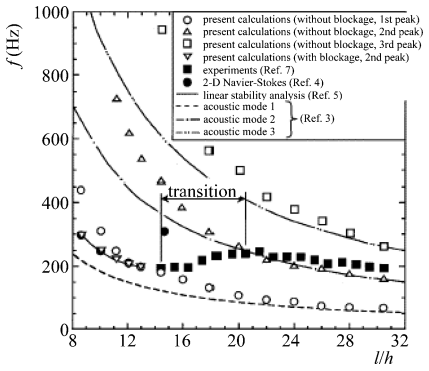

Fig. 20 Frequency vs diffuser length for Bogar experiment (Handa et al.[27]).

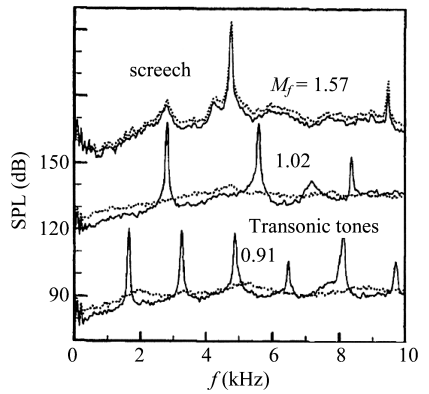

Fig. 21 Tripped boundary-layer effect (dotted lines) on resonance in sound pressure level (Zaman et al.[6]).

in the case where the effective cross-sectional area was taken into account in the calculation, an additional peak with a resonant frequency lower than 200 Hz existed. Furthermore, as shown in Fig. 20, the Bogar et al. experimental data[33] indicated that the resonant frequency variation was almost independent of the diffuser length and remained at around 200 Hz.

Contrary to Handa et al. all of these uncertainties suggest that it is unlikely that the acoustic reflection at the diffuser exit is the main mechanism for the S/S mode resonance phenomenon observed in the Bogar et al. experiment. The interaction between the turbulent boundary layer and the acoustic waves downstream of the shock as already mentioned is the most probable primary mechanism for this resonance phenomenon.

Zaman et al. in the research of C–D nozzle flows as described in Sec. II.B, showed that the acoustic resonance phenomenon was suppressed significantly by a disruption of the azimuthal coherence of the unsteadiness in the boundary layer upstream of the SIS, as shown in Fig. 21. However, note that this kind of boundary-layer disruption has to be local and azimuthally asymmetric around the nozzle, otherwise a significant coherent wave reflection could take place at the disruption ring, which can again induce resonance in the shock movement.

Robinet and Casalis[31] showed that self-excited shock oscillations could be predicted with an inviscid linear stability theory coupled with a mean flow from CFD as described in Sec. II.B. In addition, the transverse waves carried by the shear or boundary layer were not the major mechanisms for the acoustic resonance in the shock movement. However, this conclusion does not contradict the fact that longitudinal waves transmitted through the shear layer or its associated boundary layer are important for the occurrence of acoustic resonance as shown by Zaman et al.[6]

III. Supersonic and Hypersonic Nozzle Flows

The motivation of this study originated from the demand of an increase in rocket launcher performance in the area of propulsion. One of the most significant parameters for the aerodynamic performance of propulsion engines was the area ratio of the expansion nozzle situated at the base of the launcher. Increasing the area ratio could lead to a better aerodynamic performance at high altitudes but at the expense of the occurrence of unsteady flow separation inside the nozzle and, consequently, unwanted side-load effects at low altitudes. Under the ascent phase condition of the launcher, experimental data[34] indicated that, in the base region where the nozzle exit was located, a maximum rms pressure fluctuation of approximately 5% of the local mean ambient pressure occurred. For that reason, research on the generation of periodic shock motion due to the interaction between the external pressure fluctuation and the flow separation inside the nozzle was initiated.

In general, there are two kinds of flow separations inside the nozzle, FSS and RSS, as described in the Introduction. In this section, we shall review the key mechanisms or processes governing the shock wave movement inside the nozzle under the FSS flow pattern. Some of the key mechanisms or processes are similar to those already discussed in the transonic nozzle flows section. These include periodic shock motion, acoustic resonance, turbulent boundary-layer, and shear-layer instability. For high-speed nozzle flows, the following mechanisms become significant: 1) external fluctuating pressure-induced shock movement, 2) compressibility, damping and wave reflectivity, and 3) three-dimensional flow separation.

A. External Fluctuating Pressure-Induced Shock Movement

Torngren[11] conducted a series of experimental investigations with the HYP500 hypersonic wind tunnel. Preheated air at 400 K under a stagnation pressure up to 2.5 MPa with a maximum mass flow of 18 kg/s was expanded through a truncated ideal contour nozzle (known as Volvo S6). Under that condition, condensation inside the nozzle was prevented with the PR ranging from 14.5 to 59.7. The distance of L^* was 300 mm with an expansion ratio of 13.9 and an exit angle of 10.4 deg. A rotating slotted valve attached to the feeding pipe induced the fluctuating ambient pressure. The tests were conducted as a ramp-up followed by a ramp-down of nozzle feeding pressure at a constant ambient fluctuating frequency ranging between 0 and 300 Hz. The flow separation pattern under the non-full-flowing conditions was FSS type.

Torngren found that there was a strong coupling between the external flow and the flow in the separated region of the nozzle. In addition, there was amplification, up to a factor of three at $\approx$150 Hz, in the pressure fluctuation just downstream of the separation shock (P1–P5) relative to the pressure fluctuation in the external flow (P10) as shown by the profiles of the normalized pressure cross correlations at different PRs in Fig. 22. Similar amplification existed in the shock excursion corresponding to the amplification frequency in the pressure fluctuation. Moreover, the phase shift between the external pressure fluctuation and the pressure fluctuation inside the nozzle increased with the frequency, as shown in Fig. 22.

The major drawback of these experiments is the uncertainty in the symmetry of the flow separation pattern, which could have been measured if more transducers have been mounted along different axial lines inside the nozzle. Another uncertainty is the dependence of the amplification on the magnitude of the external pressure fluctuation. This uncertainty has been resolved analytically by Wong[28] (discussed subsequently) showing the independence of the amplification to the magnitude of the external pressure fluctuation.

Tijdeman[35] in his research on transonic flows around an oscillating aerofoil derived an analytical relationship between the shock movement and its downstream pressure but with an assumption of Mach number freeze as

$$\frac{\Delta p_2}{p_1} = \frac{2\gamma M_1}{\gamma+1}\left[\left\{\frac{3+\gamma-2M_1^2}{2+(\gamma-1)M_1^2}\right\}\frac{\delta M_1}{\delta x} - \frac{2i\omega}{a_1}\right]\Delta x_m e^{i\omega t} \quad (13)$$

where the first term in Eq. (13) was assumed one order-of-magnitude smaller than the second term because the Mach number freeze implied that the upstream Mach number was unchanged or changed insignificantly while the shock was oscillating. The second term

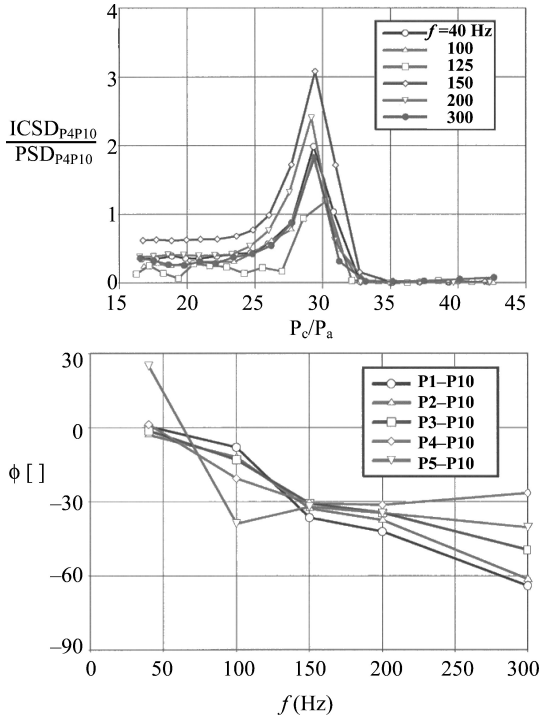

Fig. 22 Amplification and phasing between external and internal pressure fluctuations (Torngren[11]).

was in fact the velocity of the shock, which determined the pressure variation just behind shock.

Wong,[28] in the second part of his analysis on the conical shock oscillation, derived an analytical relationship between the shock excursion and its downstream pressure including the Mach number variation inside a quasi-one-dimensional conical nozzle model. The methodology was based on a Galilean transformation on the Rankine–Hugoniot relations across a shock. For a conical nozzle with a small divergent angle θ, the result yielded, as $M_1^2 \gg 1$,

$$\frac{p_2}{p_1} = \frac{2\gamma M_1^2 - (\gamma - 1)}{\gamma + 1}\left(1 - \frac{2c}{u_{10}}\right) + \mathcal{O}\left(\frac{c^2}{u_{10}^2}\right) \qquad (14)$$

which was the same as Eq. (13) obtained by Tijdeman because the first term $\delta M_1/\delta x$ was second order-of-magnitude for a small θ, which was consistent to what Tijdeman assumed.

Based on Eq. (14) and the area-ratio relation with the local Mach number combined with the one-dimensional isentropic relations for the domain upstream of the shock, Wong[28] derived a relation for the shock displacement in terms of the shock velocity, the local Mach number, and the PR across the shock.

We shall not reproduce the equation here because of its complexity but show its result on the evolution of the pressure behind shock at a frequency of 45 Hz, as shown in Fig. 23. The trajectory is very similar to the Sajben theory shown in Fig. 9. Figure 24 shows the variation of the phase angle, the shock speed, and the maximum shock displacement at different frequencies. The phase angle between the shock displacement and the pressure behind shock is shown to be asymptotic to a phase lag of 90 deg as frequency increases, independent of the amplitude of the external fluctuating pressure at the nozzle exit. This result is consistent with the result of the transonic periodic shock oscillations on a rigid airfoil based on the transonic potential theory.[36]

In addition, Wong[28] determined the amplification factor ε of the pressure just downstream of the shock based on the principle of conservation of energy applied for one period of the cycle within a control volume covering the shock excursion, as shown in Fig. 25. The quasi-one-dimensional nonlinear transport equations were solved in the subsonic domain downstream of the shock subject to the two periodic boundary conditions, one at the shock and the other at

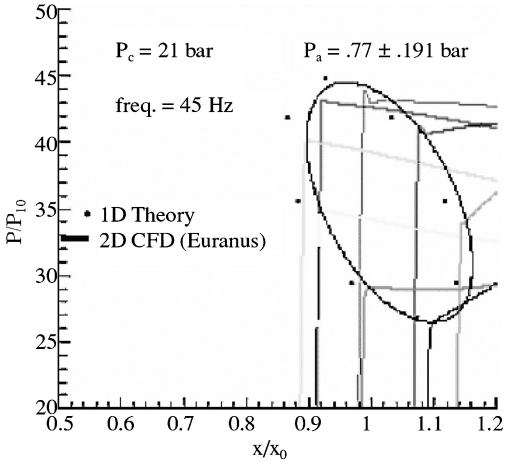

Fig. 23 Evolution of wall pressure behind shock at 45 Hz (Wong[28]).

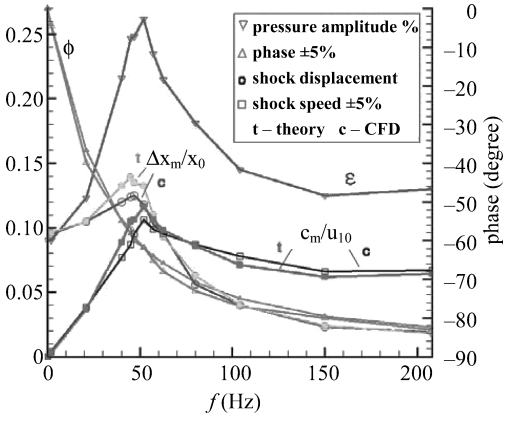

Fig. 24 Variations of phase, maximum shock displacement, and shock speed vs frequency (Wong[28]).

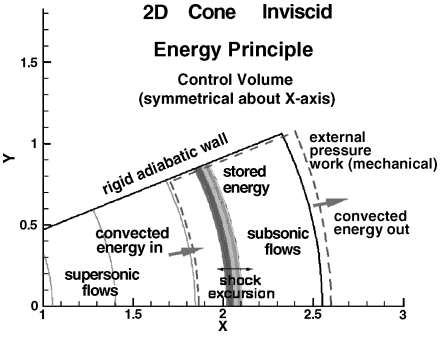

Fig. 25 Energy conservation principle applied within control volume covering the shock excursion (Wong[28]).

the nozzle exit. The resonant frequency was shown to be independent of the amplitude of the pressure fluctuation at the nozzle exit. The discrepancy at the resonant frequency was mainly caused by the higher-order effect where the function of ε was not small, as shown in Fig. 24. The frequency-dependent amplification factor ε was found to be determined mainly by the ratio of the fluctuating pressure–velocity work at the nozzle exit and the fluctuating density–velocity interaction (compression work) in the subsonic domain. The result showed that amplification factor ε was linearly proportional to the magnitude of the external pressure fluctuation ε_0, which justified the independence of the amplification (ratio of $\varepsilon/\varepsilon_0$) to the magnitude of the external pressure fluctuation in the Torngren experiment.

Furthermore, Wong[28] extended the theory of the conical nozzle to the rocket-contoured nozzle with a small divergent exit angle. Wong converted the contoured nozzle into a conical nozzle such that

Table 2 Resonant frequencies prediction at various Strouhal numbers[38]

Mode	Frequency, Hz	Strouhal	Frequency, Hz	Strouhal
0		0.06		1.633
1	12	0.071	290	1.65
2	17	0.095	320	1.89

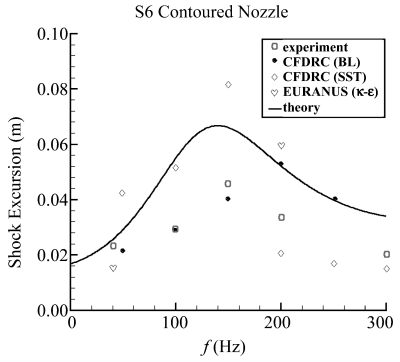

Fig. 26 Shock excursions at different frequencies (Wong[28]).

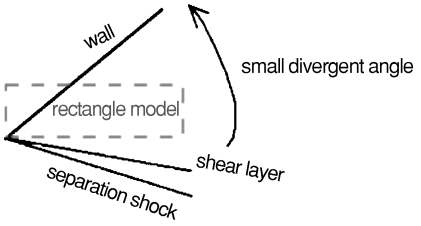

Fig. 27 Simplified two-dimensional analytical model (Sergienko and Kirillov[38]).

the separation shock could be approximated by a conical shock, but keeping the area ratio of the contoured nozzle and the location of the shock relative to the nozzle exit unchanged. The shock excursion measurement for the S6 nozzle, as reported in the experimental investigation, was compared with the theory and the CFD data from Perigo et al.,[37] as shown in Fig. 26.

The relatively larger discrepancy at higher frequencies is mainly due to the limitation of the theory for low to medium frequencies. The shock excursion from the experimental data is generally smaller than that predicted by the theory and could be attributed to the additional source in the energy dissipation due to the viscous effect ignored in the theory, including turbulence and circulation of vortices in the subsonic domain. Furthermore, there is some energy lost due to the shock- and shear-layer interaction. However, the trend in the analytical prediction is similar to those from the experimental data and the CFD results, and the resonant frequency agrees with the measurement.

Sergienko and Kirillov[38] considered the same problem as Wong[28] and analyzed the separation shock motion under the influence of an external pressure fluctuation at the nozzle exit. They designed a two-dimensional inviscid model without any limitation on the nozzle exit angle. The angle between the nozzle wall and the separation shock or the shear layer was assumed small. A restriction of $L/\lambda < \frac{1}{6}$ was imposed in which the wavelength λ was determined by the ratio of the normal component of the downstream velocity to the frequency. The Strouhal number was limited to be less than four, which implied that the model could be invalid at high frequencies. Inside the separation domain, the average velocity in the streamwise direction was assumed zero, which could be incorrect for a thick boundary layer. The two-dimensional separation domain, as shown in Fig. 27, was modeled by a rectangle through which the two-dimensional inviscid transport equations were applied. The boundary condition for the rectangle was based on some modified empirical data of nozzle pulsation loads with different shapes. Only Strouhal numbers at various frequencies of instability modes in a hot nozzle flow similar to the NASA space shuttle main engine were computed with perfect gas $\gamma = 1.2$ as shown in Table 2. The results were consistent to those observed at around 300 Hz from the space shuttle main engine during startup.

There are a number of uncertainties in the validation of this model. The angle between the wall and the shock is 19 deg, which is not small. Based on all of the research on the resonance phenomena in nozzles and diffusers as mentioned earlier, the resonant frequency is independent of the amplitude of the pulsation. Moreover, a normal shock is stable only in a divergent channel, as reported by Hurrell.[21] It is, therefore, doubtful that the pulsation correction factor can minimize the difference in the acoustic wave transport between a diverging wall domain and a uniform rectangular domain. No measurement has been taken to validate this hypothesis. Furthermore, the difference in the resonant frequency between the first and the second overtones (modes) is only 10%, which is much smaller than those differences observed in the S6 nozzle and the two-dimensional diffusers as reported earlier.

Östlund (private communication) computed the resonant frequencies for the S6 nozzle based on the theory from Sergienko and Kirillov.[38] He predicted that the fundamental mode resonant frequency at the transducer P4 was in the range of 97–127 Hz, as compared to the experimental data 150 Hz based on Fig. 22. The discrepancy was lower than expected because, under the S6 cold-flow condition, the theory limited its applicability to below 60 Hz.

Schwane et al.[4] performed numerical computations with two well-validated CFD codes, EURANUS[39] and CFD-FASTRAN,[40] to compare with the experimental data from Torngren. The first code was based on the symmetric Harten and Yee scheme with the Jameson[41] pseudotime approach augmented by several algebraic and two-equation turbulence models. The second code was based on Roe's approximate Riemann solution with the Crank–Nicholson second-order time-accurate scheme coupled with one- and two-equation turbulence models. An axisymmetric S6 nozzle configuration was used with grid refinement based on the convergence of the separation shock location. External boundary conditions were imposed to minimize the wave reflections.

Steady wall pressure profiles at different PRs were validated by the experimental data without any external pressure fluctuation. Unsteady wall pressure profiles with external pressure fluctuations at 40 and 200 Hz, shown in Fig. 28, were shown to be reasonable compared with the experimental data. However, it was unexpected to have the prediction in the amplification factor agree well with the experimental data. The turbulence model employed was not designed for such a high-frequency condition. The unsteady solutions indicated that the turbulence effects at high frequencies did not affect the amplification factor significantly apart from the mean location of the separation shock. Consequently, it was possible to have a reasonable result at least in the wall pressure downstream of the shock with a two-equation turbulence model, if the predicted mean location of the separation shock was approximately correct.

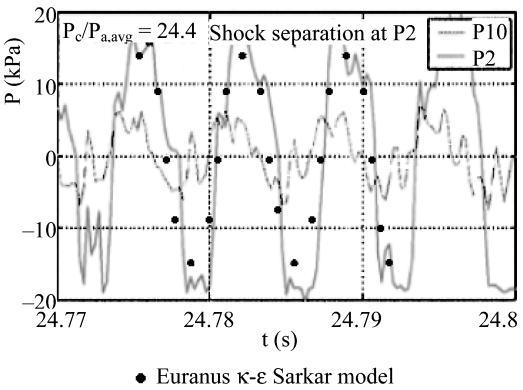

Fig. 28 Wall pressure fluctuation comparison between experiment and computation at 200 Hz; P10 external and P2 at shock, ◆, EURANUS k–ε Sarkar model (Schwane et al.[4]).

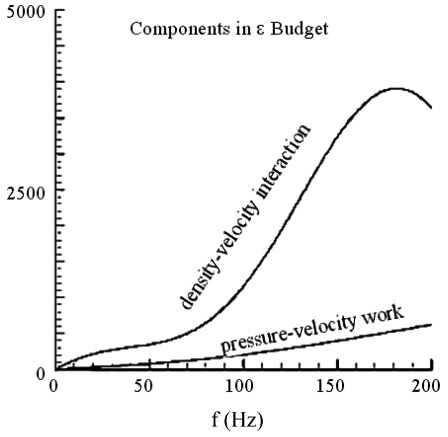

Fig. 29 Components of ε budget at different frequencies (Wong[28]).

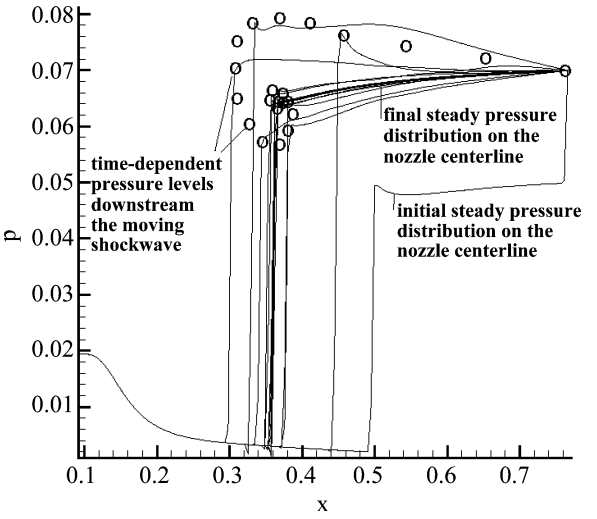

Fig. 30 Evolution of the transient behavior of a normal shock toward its equilibrium location inside a conical nozzle (Schwane et al.[4]).

B. Compressibility, Damping, and Wave Reflectivity

There are some flow similarities between the transonic C–D nozzle and the supersonic conical nozzle cases. First, the pressure at the nozzle exit fluctuates periodically at resonance as demonstrated by the CFD analysis from Loh and Zaman.[9] Second, there is a periodic shock movement as observed by Hunter[7] and Torngren.[11] Third, there is a subsonic region downstream of the shock. The main difference between the two cases is the Mach number upstream of the shock, where one is transonic or low supersonic and the other is high supersonic or hypersonic. It is mainly this difference that differentiates the amplitude and frequency of resonance in each case because of the damping due to the compressibility work as mentioned by Wong.[28] In addition, a standing wave requires a strongly reflected downstream traveling wave superimposed on the upstream traveling wave in the subsonic domain. In the supersonic or hypersonic case with a small divergent angle, the subsonic domain inside the boundary layer upstream of the shock is thin, and the wave reflectivity is in general weak because of any local asymmetrical disturbance along the circumference of the nozzle. The azimuthal coherence is disrupted. In the transonic case, the subsonic domain inside the upstream boundary layer is thick. The wave reflectivity is in general strong and not sensitive to any insignificant local disturbance. Zaman et al.[6] demonstrated this in their experimental investigation of transonic resonance with C–D nozzles under the influence of a nonuniform azimuthally tripped upstream boundary layer as shown in Fig. 21.

Moreover, in the hypersonic case where the wave reflectivity is very weak, longitudinal acoustic resonance can be overcome by the effect of amplification because of the phasing in the convective energy transported between the energy dissipation due to the shock movement and the energy supply due to external buffeting, as shown by Wong.[28] As mentioned in Sec. II.A, the amplification factor depends on the ratio of the fluctuating pressure–velocity work and the fluctuating density–velocity interaction (compression work) in the subsonic domain. The significance of the correlation between the fluctuating components of density and velocity in damping is shown in the budget of the amplification factor in Fig. 29.

These two factors, damping and wave reflectivity, significantly attenuate the amplitude of the resonance that occurs inside the subsonic domain downstream of the shock.

Schwane et al.[4] proposed that a damped linear oscillator, such as the attenuated oscillations, could model the unsteady shock movement in a one-dimensional spring–mass–dashpot mechanical system. Using CFD-FASTRAN, Schwane et al. showed that the period of oscillation was independent of its initial amplitude in the transient behavior of a conical shock settling down to its equilibrium location, after initial excitation by a sudden increase of subsonic pressure at a conical nozzle exit, as shown in Fig. 30. The evolution of the pressure just downstream of the shock along the centerline of the conical nozzle at different times showed the characteristics of the damping.

However, this only shows a necessary but not sufficient condition for a linear oscillator. Besides, the mass in this oscillation can be regarded as the periodic mass flowing through the shock, which is not a constant but is dependant on the shock velocity. Moreover, the dashpot damper depends on the periodic flow velocity as well as its correlation with the periodic density (compressibility) as shown by Wong.[28] As a first-order assessment in the case of a small cone angle, the periodic shock movement is linear, but its driving mechanism through the subsonic domain downstream of the shock is nonlinear.

C. Three-Dimensional Flow Separation

Many researchers in the last decade investigated unsteady side-loads acting on a nozzle as a consequence of the movement of a three-dimensional separation shock with a developed separation zone. The transient side-loads generated in these cases are either due to the transition from one kind of separation pattern to another (FSS–RSS)[10,42] within a short duration, or as a result of pressure fluctuations[43,44] inside the nozzle that are related to turbulence, including the shock and boundary-layer interaction. This short duration takes place during the startup or the shutdown phase of the nozzle engine and is at least one order-of-magnitude shorter than the timescale for the existence of the periodic shock motion mentioned earlier. The separation shocks in these cases are in general asymmetrically three dimensional, as experimentally observed by Verma and Ciezki,[45] and the mechanisms are not acoustic related. The approach is semi-empirical, based on the statistical characteristics of the pressure distribution inside the nozzle measured by experiments.

Deck et al.[46] showed in a three-dimensional CFD computation with FLU3M[47] and elsA,[48] and confirmed with oil-flow visualizations, the influence of the side walls to the flow manifesting the occurrence of a three-dimensional flow separation inside the two-dimensional diffuser in the S8Ch wind tunnel at ONERA. The skin-friction lines over the side, the lower, and the upper walls, indicating the separation and reattachment lines and the footprints of the vortices rolling up in the separation domain, were computed, as shown in Fig. 31. In addition, the Laboratoires d'Études Aérodynamiques (LEA), Poitiers, France, axisymmetric truncated ideal contour (TIC) nozzle was computed, which again indicated a three-dimensional flow separation inside the nozzle, as shown in Fig. 32.[49]

However, it remains unclear whether the unsteady turbulent shear layer that emanates from the separation shock causing pressure pulsations in the separation domain is the driving mechanism for this three-dimensional flow separation phenomenon, or if it is related to the unsteadiness in the PR, or is a combination of both. Three-dimensional flow separation can also be induced by nonuniform azimuthally varied external pressure fluctuations at the nozzle exit. Nevertheless, this shows the uncertainty of the symmetry assumption in the analysis of the periodic shock motion.

IV. Other Complex Nozzle Flows

It may be useful to highlight the major differences between the screech and the nonscreech tones in transonic or supersonic nozzle flows. In general, screech tones take place externally outside a nondivergent nozzle, for example, a rectangular nozzle with a beveled exit. Nonscreech transonic tones take place internally inside of a simple C–D nozzle. Screech tones associate with different phases in the transverse direction, independent of Mach number, whereas in the nonscreech case, an axisymmetric same phase exists for a certain range of Mach numbers. Jet Mach number is defined as the ideal one-dimensional inviscid Mach number M_j at the nozzle exit without separation. The resonant frequency in screech tones decreases with the jet Mach number increases, whereas in the nonscreech case, the resonant frequency increases with the jet Mach number, as shown in Fig. 7. The dominant mode in amplitude is not necessarily the lowest-order mode in the screech case. This indicates that the mechanisms for the generation of these two phenomena are quite different. The noise level is also a bit louder in the nonscreech transonic tones than in the screech tone. Moreover, the tripped boundary-layer effect can influence the occurrence of resonance significantly in the nonscreech transonic tones but not at all in the screech tone, as shown in Fig. 21. This demonstrates that the resonance in the screech tone is based on the external acoustics and is independent of the azimuthal coherence of the unsteadiness inside the nozzle.

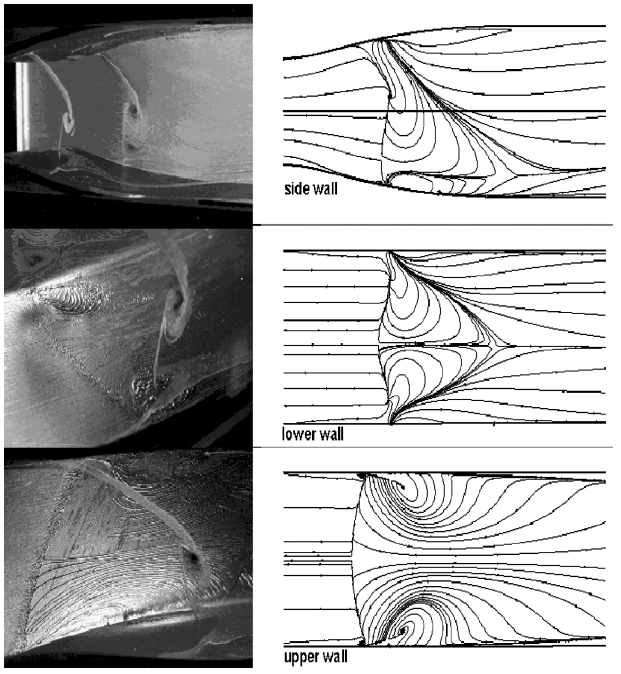

Fig. 31 Skin-friction lines indicating three-dimensional flow separation inside two-dimensional diffuser in S8Ch wind tunnel (Deck et al.[46]).

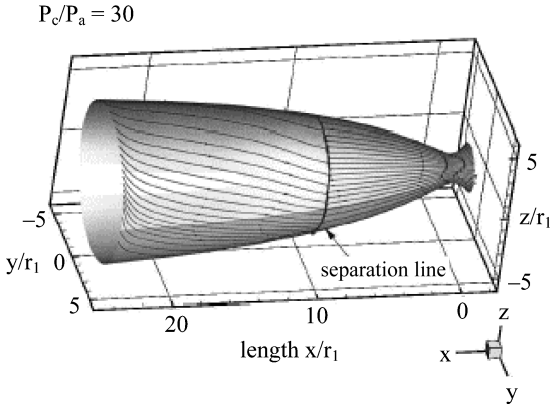

Fig. 32 Skin-friction lines indicating three-dimensional flow separation inside axisymmetric TIC nozzle at LEA (Deck et al.[49]).

Finally, the whistler-nozzle phenomenon occurs from the coupling of two independent resonance mechanisms: 1) the shear-layer tone resulting from the impingement of the pipe-exit shear layer on the collar lip attached to the end of the pipe nozzle and 2) the pipe resonance similar to the nonscreech transonic tone but at a subsonic speed. Unlike the other tones, the whistler-nozzle excitation does not depend on the streamwise velocity explicitly, but rather on the matching of the shear-layer tone frequency to one of the pipe resonant frequencies. This implies the existence of a dead zone, where the conditions for both resonance mechanisms cannot be simultaneously met.

Table 3 summarizes all of the mechanisms mentioned in this paper. The levels of strong, medium, and weak represent relative strengths compared with other effects, and the level in each case should not be regarded as the strength of the effect. In general, acoustics are relatively weak in supersonic flows and strong in subsonic flows, compared with other effects. The turbulence effect depends on its frequency matching with the shock resonant frequency. Based on the data available at present, the amplification is classified as low at around 2–3 and as high at 10 or above.

V. Conclusions

An overview of some of the flow oscillation phenomena occurring inside nozzles and diffusers with a small divergent angle and a flow speed ranging from transonic to hypersonic has been presented. Based on all of the research reported in this paper, including investigations from experimental data, CFD solutions, and theoretical studies, the major conclusions from this overview, for low to medium frequencies, can be summarized as follows.

1) With a no separation or PGIS mode, the shock acts to dissipate acoustic energy by attenuating oscillations.

2) With an SIS mode, the shock behaves to drive the oscillations, inducing λ shocks formation.

3) The amplitude of resonance is attenuated by the damping and wave reflectivity inside the subsonic domain downstream of the separation shock.

4) Damping can be caused by compressibility work and turbulence dissipation inside the subsonic domain.

5) Disruption of the azimuthal coherence in the subsonic boundary layer upstream of the separation shock attenuates the wave reflectivity.

Table 3 Physical mechanisms for resonance phenomena in nozzle flows

Mach upstream	Acoustics: Shear-layer instability[a]	Acoustics: Wave reflectivity[b]	Acoustics: Damping[c]	Turbulence fluctuation	External of buffeting relative to acoustics	Multiple resonances	Amplification factor	Example
Subsonic	Strong	Strong	Weak	Weak	Weak	Medium (internal)	High	Whistler nozzle
Transonic	Medium	Medium	Medium	Weak–Strong (amplitude and frequency)	Medium	Weak	Medium	C–D diffuser/nozzle
Supersonic	Weak	Weak	Strong	Weak–Strong (amplitude and frequency)	Strong	Weak/strong (external)	Low	TIC nozzle/ rectangular nozzle

[a]Compressibility-flow correlations.
[b]Azimuthal coherence, subsonic boundary-layer thickness and turbulence blockage.
[c]Compressible flow correlation, shear-layer instabilities (transversal), and turbulence dissipation.

6) The resonant frequency is mainly governed by the characteristic length scale defined as the distance between the separation shock and the location where acoustic reflections occur.

7) The characteristic length scale is influenced by the PR, turbulent boundary layer, Reynolds effect, and nozzle divergence, angle in addition to the nozzle length.

8) Longitudinal waves initiated at the subsonic stems of the separation shock (self-excited) or at the nozzle exit (external buffeting) are the sources of generating acoustic resonance.

9) The superposition of upstream and downstream traveling waves inside the subsonic domain generates the acoustic resonance.

10) Weak resonance (amplification) can be induced by the phasing in the convective energy transported between the energy dissipation due to shock movement and the energy supply due to external buffeting.

11) Asymmetric acoustic resonance occurs mainly in a nondivergent or complex geometry nozzle, and its mechanism is associated with external acoustics.

It remains unclear under what physical conditions an asymmetric acoustic resonance in nonscreech tones can occur. The significance of the complexity in the shock structures and its interactions with the subsonic boundary layer, to the degree of reflectivity (amplitude) of the disturbances propagating upstream and downstream inside the subsonic domain, requires further investigational research.

Acknowledgments

A part of this work has been performed within the framework of the European Flow Separation Control Device (FSCD) Working Group. The author is deeply indebted to FSCD colleagues for many fruitful discussions and valuable comments. The author gratefully acknowledges the support and kind permission to reproduce the figures from many international colleagues mentioned in this paper. Encouragement and technical support from the colleagues in the European Space Technology and Research Center, especially Richard Schwane, Wilhelm Kordulla, and Jean Muylaert are sincerely appreciated.

References

[1]Hill, W., and Greene, P., "Increased Turbulent Mixing Rates Obtained by Self-Excited Acoustic Oscillations," *Journal of Fluids Engineering*, Vol. 99, 1977, pp. 520–545.

[2]Krothapalli, A., and Hsia, Y., "Discrete Tones Generated by a Supersonic Jet Ejector," *Journal of Acoustic Society America*, Vol. 99, 1996, pp. 777–784.

[3]Mabey, D., *Physical Phenomena Associated with Unsteady Transonic Flows*, Progress in Astronautics and Aeronautics, Vol. 120, AIAA, Washington, DC, 1989, pp. 1–56.

[4]Schwane, R., Wong, H., and Torngren, L., "Validation of Unsteady Turbulent Flow Predictions for Over-Expanded Rocket Nozzles," *Proceedings of International Conference in CFD2*, Springer-Verlag, Berlin, 2002, pp. 707–712.

[5]Culick, F., "Oscillatory and Unsteady Processes in Liquid Rocket Engines," *Proceedings of Combustion Instability in Liquid Rocket Engines*, ESA Rept., WPP-062, Noordwijk, The Netherlands, Sept. 1993.

[6]Zaman, K., Dahl, M., Bencic, T., and Loh, C., "Investigation of a 'Transonic Resonance' with Convergent–Divergent Nozzles," *Journal of Fluid Mechanics*, Vol. 463, 2002, pp. 313–343.

[7]Hunter, C., "Experimental Investigation of Separated Nozzle Flows," *AIAA Journal*, Vol. 20, No. 3, 2004, pp. 527–532.

[8]Sajben, M., and Kroutil, J., "Effects of Initial Boundary-Layer Thickness on Transonic Diffuser Flows," *AIAA Journal*, Vol. 19, No. 11, 1980, pp. 1386–1393.

[9]Loh, C., and Zaman, K., "Numerical Investigation of Transonic Resonance with a Convergent–Divergent Nozzle," *AIAA Journal*, Vol. 40, No. 12, 2002, pp. 2393–2401.

[10]Frey, M., and Hagemann, G., "Restricted Shock Separation in Rocket Nozzles," *Journal of Propulsion and Power*, Vol. 16, No. 3, 2000, pp. 478–484.

[11]Torngren, L., "Correlation Between Outer Flow and Internal Nozzle Pressure Fluctuations," *Proceedings of the 4th European Symposium on Aerothermodynamics for Space Vehicles*, ESA, Noordwijk, The Netherlands, 2001, pp. 415–424.

[12]Hussain, A., and Hasan, M., "The 'Whistler-Nozzle' Phenomenon," *Journal of Fluid Mechanics*, Vol. 134, 1983, pp. 431–458.

[13]Raman, G., "Advances in Understanding Supersonic Jet Screech: Review and Perspective," *Progress in Aerospace Sciences*, Vol. 34, Jan. 1998, pp. 45–106.

[14]Chen, P., Sajben, M., and Kroutil, C., "Shock-Wave Oscillations in a Transonic Diffuser Flow," *AIAA Journal*, Vol. 17, No. 10, 1979, pp. 1076–1083.

[15]Bogar, J., Sajben, M., and Kroutil, C., "Characteristic Frequencies of Transonic Diffuser Flow Oscillations," *AIAA Journal*, Vol. 21, No. 9, 1983, pp. 1232–1240.

[16]Meier, G., "Shock Induced Flow Oscillations," *AGARD Proceedings in Flow Separation*, No. 168, 1974.

[17]Szumowski, A., Obermeier, F., and Meier, G., "Oscillation Modes of Laval Nozzle Flow," *Experiment in Fluids*, Vol. 18, Springer-Verlag, Berlin, 1995, pp. 145–152.

[18]Ishibashi, M., and Takamoto, M., "Discharge Coefficients of Critical Nozzles with Step near the Throat and Their Flowfield Estimated from Recovery Temperature Distribution," *Proceedings of ASME FEDSM'01*, FEDSM2001-18035, American Society of Mechanical Engineers, New York, 2001.

[19]Burgers, J., "On the Transmission of Sound Waves Through a Shock Wave," *Proceedings, Koninklijke Nederlandse Akademie van Wetenschappen*, Vol. 49, No. 3, 1946, pp. 274–281.

[20]Kantrowitz, A., "The Formation and Stability of Normal Shock Waves in Channel Flows," NACA TN 1225, Nov. 1946.

[21]Hurrell, H., "Analysis of Shock Motion in Ducts During Disturbances in Downstream Pressure," NACA TN 4090, July 1957.

[22]Wasserbauer, J., and Walloh, R., "Experimental and Analytical Investigation of the Dynamic Response of a Supersonic Mixed Compression Inlet," AIAA Paper 68-651, June 1968.

[23]Richey, G., and Adamson, T., Jr., "Analysis of Unsteady Transonic Channel Flow with Shock Waves," *AIAA Journal*, Vol. 14, No. 8, 1976, pp. 1054–1061.

[24]Adamson, T., Messiter, A., and Liou, M., "Large Amplitude Motion in Two-Dimensional Transonic Channel Flows," *AIAA Journal*, Vol. 16, No. 12, 1978, pp. 1240–1247.

[25]Culick, F., and Rogers, T., "Response of Normal Shocks in Diffusers," *AIAA Journal*, Vol. 21, No. 10, 1983, pp. 1382–1390.

[26]Sajben, M., "Response of Normal Shocks in Diffusers," *AIAA Journal*, Vol. 23, No. 3, 1985, pp. 477–478.

[27]Handa, T., Masuda, M., and Matsuo, K., "Mechanism of Shock Wave Oscillation in Transonic Diffusers," *AIAA Journal*, Vol. 41, No. 1, 2003, pp. 64–70.

[28]Wong, H., "Theoretical Prediction of Resonance in Nozzle Flows," *Journal of Propulsion and Power*, Vol. 21, No. 2, 2005, pp. 300–313.

[29]Liou, M., and Coakley, T., "Numerical Simulation of Unsteady Transonic Flow in Diffusers," *AIAA Journal*, Vol. 22, No. 8, 1984, pp. 1139–1145.

[30]Hsieh, T., and Coakley, T., "Downstream Boundary Effects on the Frequency of Self-Excited Oscillations in Transonic Diffuser Flows," AIAA Paper 87-0161, Jan. 1987.

[31]Robinet, J.-C., and Casalis, G., "Shock Oscillations in Diffuser Modeled by a Selective Noise Amplification," *AIAA Journal*, Vol. 37, No. 4, 1999, pp. 453–459.

[32]Yee, H., "Upwind and Symmetric Shock-Capturing Schemes," NASA TM 89464, 1987.

[33]Bogar, J., Sajben, M., and Kroutil, C., "Characteristic Frequencies and Length Scales in Transonic Diffuser Flow Oscillations," AIAA Paper 81-1291, June 1981.

[34]Meijer, J., and van Beek, C., "Analysis of Ariane5 Base Flow Measurements in the NLR/PHST and FFA/T1500 Wind Tunnels," National Aerospace Lab., Rept. NLR-CR-99449, Amsterdam, Nov. 1999.

[35]Tijdeman, H., "Investigation of the Transonic Flow Around Oscillating Aerofoils," National Aerospace Lab., Rept. TR-77-090U, Amsterdam, The Netherlands, 1977.

[36]Nixon, D., *Unsteady Transonic Aerodynamics*, Progress in Astronautics and Aeronautics, Vol. 120, 1989, AIAA, Washington, DC, pp. 13, 71.

[37]Perigo, D., Schwane, R., and Wong, H., "A Numerical Comparison of the Flow in Conventional and Dual-Bell Nozzles in the Presence of an Unsteady External Pressure Environment," AIAA Paper 2003-4731, July 2003.

[38]Sergienko, A., and Kirillov, A., "Pulsating Loads on Propulsive Nozzles with Flow Separation," *Aviatsionnaya Tekhnika* Ref No. 0579-2975, No. 4, 2000, pp. 23–26.

[39]Eliasson, P., and Nördstrom, J., "The Development of an Unsteady Solver for Moving Meshes," Swedish Defence Agency, Stockholm, TN 1995-39, 1995.

[40]Coirier, W., and Bayyuk, S., "Modeling of Blast Waves in Urban Areas Using Hierarchical, Adaptive Mesh Refinement," AIAA Paper 2002-2749, June 2002.

[41]Jameson, A., "Time Dependent Calculations Using Multi-grid with Applications to Unsteady Flows past Airfoils and Wings," AIAA Paper 91-1596, June 1991.

[42]Hagemann, G., Terhardt, M., Frey, M., Reijasse, P., Onofri, M., Nasuti, F., and Östlund, J., "Flow Separation and Side-loads in Rocket Nozzles," *4th International Symposium on Liquid Space Propulsion*, A620393, German Aerospace Center, Lampoldshausen, Germany, Aug. 2000.

[43]Dumnov, G., "Unsteady Side-loads Acting on the Nozzle with Developed Separation Zone," AIAA Paper 96-3220, July 1996.

[44]Kistler, M., "Fluctuating Wall Pressure Under a Separated Supersonic Flow," *Journal of the Acoustical Society of America*, Vol. 36, No. 3, 1966.

[45]Verma, S., and Ciezki, H., "Unsteady Nature of Flow Separation Inside a Thrust Optimized Parabolic Nozzle," AIAA Paper 2003-1139, Jan. 2003.

[46]Deck, S., Hallard, R., and Guillen, P., "Numerical Simulations of Steady and Unsteady Separated Nozzle Flows," AIAA Paper 2002-0406, Jan. 2002.

[47]Péchier, M., "Prévisions numériques de l'effet Magnus pour des configurations de munition," Ph.D. Dissertation, Aerodynamics Dept., Univ. de Poitiers, Poitiers, France, 1999.

[48]Cambier, L., and Gazaix, M., "An Efficient Object-Oriented Solution to CFD Complexity," AIAA Paper 2002-0108, Jan. 2002.

[49]Deck, S., and Guillen, P., "Numerical Simulation of Side Loads in an Ideal Truncated Nozzle," *Journal of Propulsion and Power*, Vol. 18, No. 2, 2002, pp. 261–269.